Article

Stimuli-Responsive Templated Polymer as a Target Receptor for a Conformation-Based Electrochemical Sensing Platform

Habib M. N. Ahmad, Gaurab Dutta, John Csoros, Bo Si, Rongfang Yang, Jeffrey M. Halpern, W. Rudolf Seitz, and Edward Song*

Cite This: https://dx.doi.org/10.1021/acsapm.0c01120

Read Online

ACCESS | ihl Metrics & More | 📰 Article Recommendations | 🟦 Supporting Information

ABSTRACT: The use of highly cross-linked molecularly imprinted polymers as a synthetic target receptor has the limitations of restricted accessibility to the binding sites, resulting in a slow response time. Moreover, such artificial receptors often require additional transduction mechanisms to translate target binding events into measurable signals. Here, we propose the development of a single-chain stimuli-responsive templated polymer, without using any covalent interchain cross-linkers, as a target recognition element. The synthesized polymer chain exhibits preferential binding with the target molecule with which the polymer is templated. Moreover, upon specific target recognition, the polymer undergoes conformation change induced by its particular stimuli responsiveness, namely, the target binding event. Such templated single-chain polymers can be attached to the electrode surface to implement a label-free electrochemical sensing platform. A target analyte, 4-nitrophenol (4-NP), was used as a template to synthesize a poly(N-isopropylacrylamide) (PNIPAM)-based copolymer chain which was anchored to the electrode to be used as a selective receptor for 4-NP. The electrode surface chemistry analysis and the electrochemical impedance study reveal that the polymer concentration, the interchain interactions, and the Hofmeister effect play a major role in influencing the rate of polymer grafting as well as the morphology of the polymers grafted to the electrode. We also show that the specific binding between 4-NP and the copolymer results in a substantial change in the charge transfer kinetics at the electrode signifying the polymer conformation change.

KEYWORDS: poly(N-isopropylacrylamide), stimuli-responsive, molecular imprinting, electrochemical sensing, nitrophenol, conformation change, templated polymer, RAFT
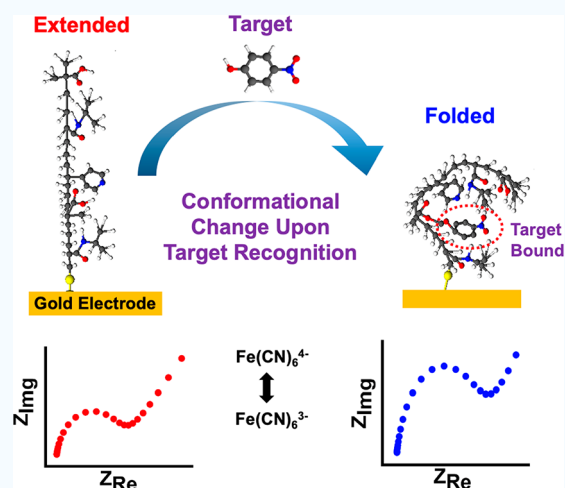
INTRODUCTION

Molecular templating, also known as molecular imprinting, is a promising technology for creating artificial and synthetic receptors for the recognition of target species.[1−3] A molecularly templated polymer is created by synthesizing a polymer matrix in the presence of the templating molecule (i.e., the analyte) such that the polymer will capture the unique molecular features of the template, thereby creating a molecular cavity that is complementary in structure to the template molecule. This templated polymerization is performed with the anticipation that the polymer would exhibit preferential binding to the template molecule compared to other nonspecific molecules that may be regarded as interfering species.

Traditionally, molecularly imprinted polymers developed for sensing applications were based on a highly cross-linked polymer matrix with the imprinted molecular cavities buried in the bulk of the material.[4] However, highly cross-linked polymers tend to limit the target species from accessing the

recognition sites, especially when the analyte is large in molecular weight. Templating of epitopes has also been demonstrated where the recognition sites are partially open, allowing easy access to the receptors.[5,6] Typically, in this framework, the binding event between the target and the polymer-based binding site must be accompanied by a secondary transduction mechanism (such as optical, electrochemical, and mass sensing).[2,7−9] Additionally, highly cross-linked polymers tend to be rigid, resulting in slow capture and release of the target, and therefore may not be the desired platform for continuous and real-time detection. Therefore, as

A
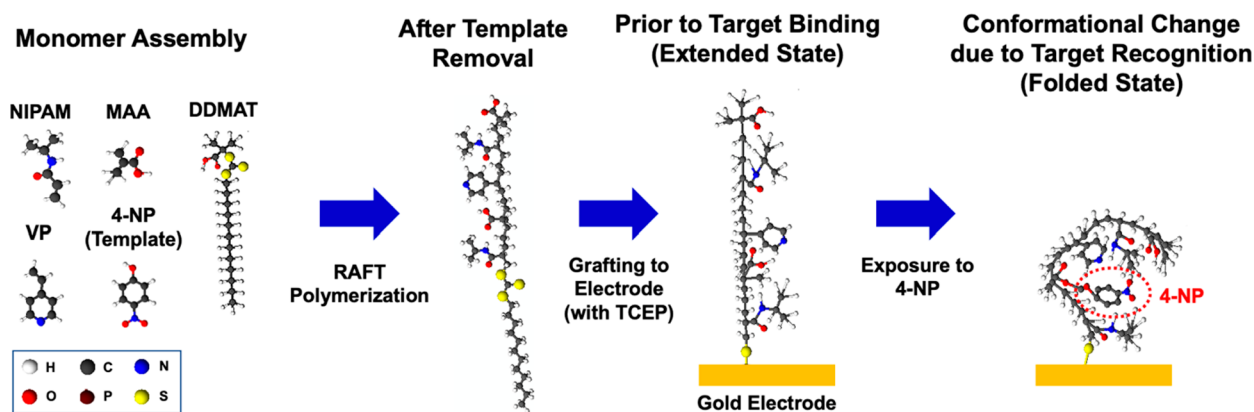
Figure 1. Conceptual illustration of the synthesis of a single-chain PNIPAM-based templated copolymer as a receptor for the target 4-nitrophenol (4-NP) and its use as a conformation-dependent electrochemical sensor.

an alternative approach, loosely cross-linked polymers have been considered for creating a templated target receptor.

Previously, Watanabe et al. have prepared templated polymers using only 5 mol % cross-linking with poly(N-isopropylacrylamide) (PNIPAM) as the backbone polymer, resulting in a hydrogel that either swells or shrinks depending on the number of template molecules bound.[10] PNIPAM is a well-known stimuli-responsive polymer with a lower critical solution temperature (LCST) of ~32 °C.[11−13] If comonomers are incorporated into the PNIPAM backbone, the LCST shifts either higher or lower depending on whether the comonomer is hydrophilic or hydrophobic. The volume of the templated PNIPAM gel above LCST was found to increase with increasing concentration of the template molecules (non-templated hydrogels had no template-dependent volume change). This finding suggests that it is possible to obtain selective binding by templated polymers even with low percentage of covalent cross-linkers and that there are other forms of cross-linking that help preserve the conformation of the template binding sites. We have hypothesized that such cross-linking comes from the noncovalent hydrophobic interactions between the isopropyl groups in PNIPAM. Furthermore, the observation that hydrogel volume change depends on the template concentration suggests that template binding affects the conformation of the polymer. We exploit this effect in the work reported here as well.

More recently, a fluorescein-templated copolymer with only 2 mol % covalent cross-linker was developed by the Seitz group.[14] The formulation included PNIPAM as the backbone with methacrylic acid (MAA) and vinylpyridine (VP). The MAA and VP monomers formed acid−base cross-links to help retain polymer conformation to make up for the lack of covalent cross-links. The binding constant (K_a) for this copolymer binding with fluorescein was measured to be 3×10^8 M^{-1}, much larger than that of typical molecularly imprinted polymers. The response time was also much faster with the templated polymer binding to the target in less than 1.5 s, orders of magnitude faster than a typical templated polymer with a high degree of covalent cross-linking. When the polymer was templated with 4-nitrophenol (4-NP), by using fluorescence quenching as a readout, the polymer showed promising selectivity toward 4-NP and minimum interaction with its isomers 2-NP and 3-NP.[15] Similar selectivity was also demonstrated for polymers templated with 3-NP. Furthermore, the conformational changes in the polymer upon template

binding has been confirmed by using the fluorescence resonance energy transfer (FRET) donor−acceptor interaction.[15] However, electrochemical sensing with this type of templated polymer has not been demonstrated so far.

Building on these previous works, we propose a new approach to molecular templating by fully eliminating covalent cross-linkers and using a single-chain polymer as a target receptor. We have also implemented an electrochemical sensing platform by grafting the single-chain templated polymers to the electrode surface. We hypothesized that the templated single-chain PNIPAM-based polymer would selectively recognize the target with reasonable affinity, and upon target binding, the polymer will undergo its conformation change as a result of its stimuli responsiveness. This sensing platform was inspired in part by the aptamer-based target detection from the Plaxco group, whereby the single-stranded DNA or RNA oligonucleotide sequence undergoes conformation change upon target recognition, which can then be used as a transduction mechanism for label-free sensing.[16] In our synthetic target receptor, the conformation of the single-chain templated polymer changes from an extended random coil to a folded structure when the target is bound.[17] Moreover, such polymers can be attached to the electrode surface to implement electrochemical impedance-based sensors.

In this work, we employed PNIPAM copolymerized with functional monomers MAA and VP to form a single-chain templated polymer to create a synthetic target receptor for the detection of 4-nitrophenol (4-NP) based on previous developments.[14,15,18] Figure 1 illustrates the overview of the proposed sensing platform including polymer synthesis, electrode modification, and target recognition. The target molecule 4-NP is a toxic chemical that can significantly damage human health, including damages to the liver and kidney. Identified as a priority pollutant by the United States Environmental Protection Agency, 4-NP is also known to cause lethargy, headaches, and cyanosis in humans.[19] Furthermore, 4-NP also acts as a biomarker present in urine when exposed to methyl parathion, an organophosphate pesticide that is prohibited for use in the United States.[20] Therefore, the detection of 4-NP is of critical importance for human and environmental health. Sherrington et al. have previously demonstrated that MAA and VP can serve as functional monomers for the detection of 4-NP with high affinity.[21,22] In the proposed sensor platform, the conformation change of the templated polymer upon binding with 4-NP affects the electrochemical impedance at the
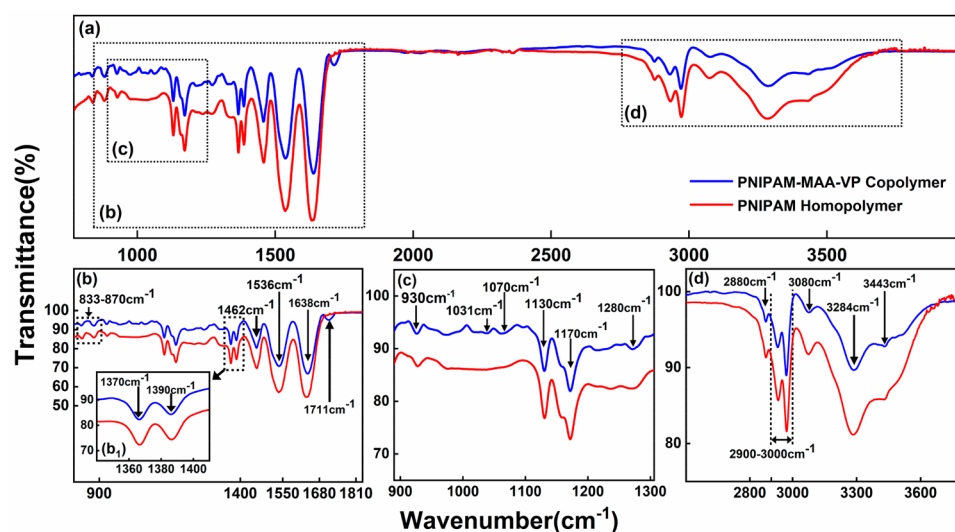
Figure 2. Fourier transform infrared (FTIR) spectra comparison between the PNIPAM−MAA−VP copolymer (blue) and the PNIPAM homopolymer (red). The overall FTIR spectra for both samples are shown in (a) with select regions magnified in the insets (b−d).
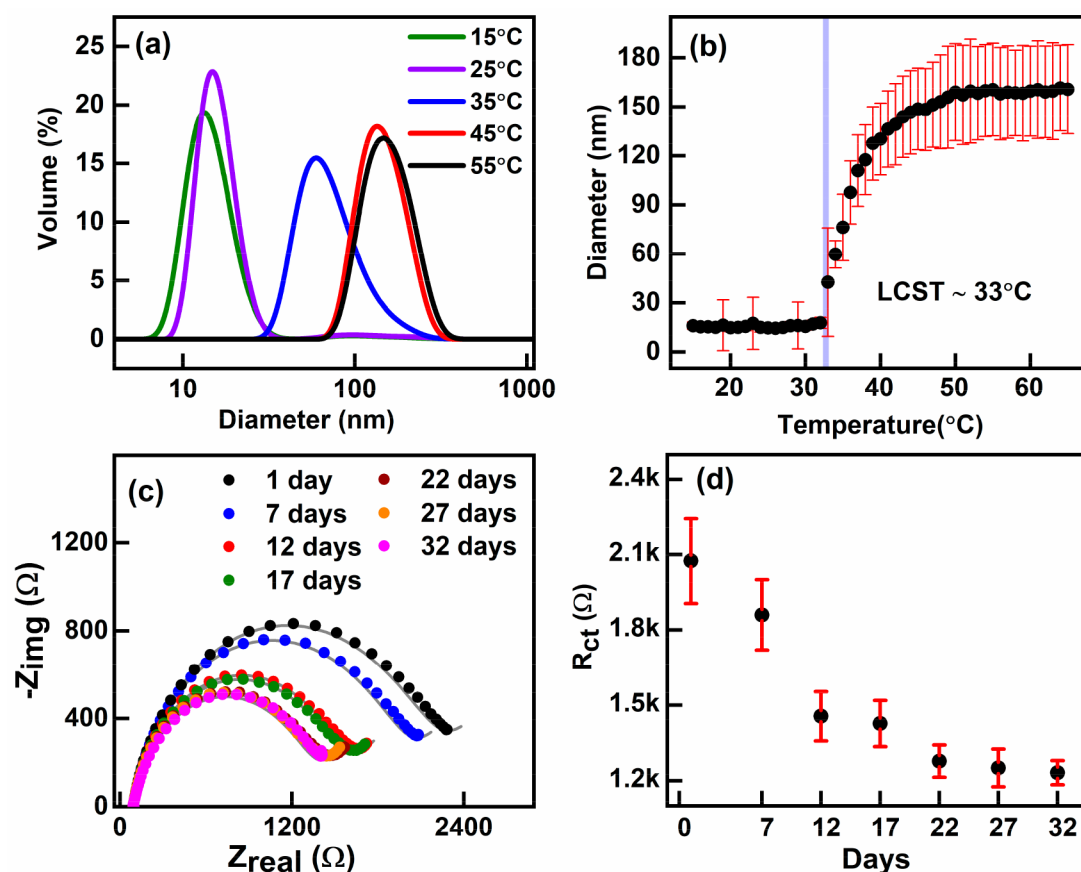
Figure 3. Characterization of the temperature- and time-dependent polymer dispersion in solution. (a) Distribution of the hydrodynamic radius (D_h) of the polymers at different temperatures measured via dynamic light scattering (DLS) in MOPS buffer (pH 7). Legends: 15 °C (purple), 25 °C (green), 35 °C (blue), 45 °C (red), and 55 °C (black). (b) Average diameter of the polymer sample as a function of temperature. The diameter is taken at the maximum volume percentage point from the DLS measurements. The vertical line indicates the lower critical solution temperature (LCST). Measurements were repeated three times ($n = 3$). (c) Nyquist plot of the polymer-attached gold electrode as a function of time. (d) Plot of charge transfer resistance (R_{ct}) as a function of time ($n = 3$).

electrode surface, which is used as a readout for the 4-NP detection. In addition to the polymer synthesis and characterization, the polymer surface coverage on the electrode, the binding kinetics, and the hydration effects are also studied.

■ **RESULTS AND DISCUSSION**

Synthesized Polymer Compositional Characterization via FTIR and NMR. The templated polymers were synthesized by using the RAFT (reversible addition−

fragmentation chain transfer) polymerization method since it is a highly controllable radical polymerization process that leads to high polymer integrity and low polydispersity index.[23,24] To verify the compositional integrity, the PNIPAM copolymerized with functional monomers, methacrylic acid (MAA) and 4-vinylpyridine (VP), was compared with pure PNIPAM homopolymer by using FTIR. Both polymers were synthesized to have an average chain length of 100-mers. The FTIR spectra in Figure 2 show that a significant portion of vibrations arises from PNIPAM and the RAFT chain transfer agent DDMAT (2-dodecylthiocarbonothioylthio-2-methylpropionic acid) present in both homopolymer and copolymer samples. The FTIR also confirms that the peaks associated with MAA and VP are only present in the copolymer and not in the homopolymer. The details of the FTIR peak analysis is provided in the Supporting Information (section 1).

The degradation or thermooxidation of monomers such as NIPAM, MAA, and VP in the copolymer may cause the polymer chain scission during the polymerization. The carbonyl index (CI) of the polymer provides a relative estimation of the evolution of carbonyl functionalities. The fluctuations of the carbonyl group in the polymer chain can be influenced by various phenomena (e.g., evaporation, photo-oxidation, and leaching). Such unwanted scenarios can occur during RAFT and the lyophilization processes. The CI qualitatively assesses the polymer backbone scission in the chain.[25] It was estimated by the formula $CI = \frac{A_{1638/1636 \text{ cm}^{-1}}}{A_{1462 \text{ cm}^{-1}}}$, where $A_{1638 \text{ cm}^{-1}}$, and $A_{1462 \text{ cm}^{-1}}$ are the absorbances (absorbance: $A = 2 - \log(\%T)$). The CI values were ~2.0 for the homopolymer and ~1.8 for the copolymer. Such carbonyl indices indicate successful RAFT polymerization processes without a significant unwanted degradation in compositional monomers in a polymer chain of approximately 100-mer length for both samples.[25]

The presence of the RAFT chain transfer agent (DDMAT), MAA, and VP in the copolymer was also verified with NMR. For further confirmation, the NMR measurement was conducted on both the homopolymer and the copolymer. The NMR analysis (detailed in the Supporting Information, section 1) confirms the compositional elements and their molar ratios of the copolymer. Furthermore, it also confirms the estimated 100-mer average length of the polymer chain for both samples.

Study of Dispersion, LCST, and Dynamic Aggregation of the PNIPAM Copolymer via Dynamic Light Scattering (DLS) Measurements. The dynamic light scattering (DLS) measurements reveal the temperature dependency of the conformations of PNIPAM-based copolymers as well as their interactions with the neighboring polymers. The phase transformation and aggregation of PNIPAMs due to the intermolecular forces such as the hydrophobic interaction and hydrogen bonding are well documented.[12−14,26−29] Figure 3a shows the DLS volume percentage curves as a function of the particle size. At low temperatures (15−25 °C), a peak near 10−30 nm appears due to the possible presence of micelles formed by the PNIPAM chains.[30] However, for temperatures above 35 °C, the average diameter of the particles increases, suggesting a greater agglomeration of polymers at high temperatures. Hore and co-workers have suggested that dodecane-terminated PNIPAM homopolymers form smaller agglomerations (of ~20 nm in size) below LCST in the aqueous solution.[28] Epps III and O'Reilly et al. have also

shown that above the critical micelle concentration (0.01 mg/mL) the DDMAT-terminated PNIPAM homopolymers form a complex assembly of micelles (both cylindrical and spherical structured) caused by the dodecane chain.[31] They have also reported that the hydrodynamic diameter (D_h) of the majority of the micelles varied between 10 and 20 nm (consistent with our DLS measurements) with some population of larger aggregates ($D_h \sim 200$ nm) in aqueous media. It is worth noting that the larger sized aggregations cause a greater degree of light scattering and therefore lead to a higher DLS intensity compared to that of the smaller sized micelles.[26,29,32] Therefore, the DLS volume percentage plot as shown in Figure 3a rather than the intensity plot is a more accurate representation of the population (or the percentage makeup) of the given particle size.

The particle sizes greater than 10 nm indicate that most copolymer chains are water-soluble due to the hydrated state of PNIPAM via hydrogen bond formation between the amide groups in the polymer and water molecules. Such hydration is reasonable at the buffer concentrations at or below 0.5 M.[26] Figure 3a shows that as the temperature increases above the LCST (35−55 °C), the size of the aggregates is in the range 50−300 nm, which indicates significant hydrophobic inter-chain interactions among the polymer chains.[26,33]

From Figure 3b, the LCST of the PNIPAM−MAA−VP copolymer estimated is ~33 °C, slightly higher than that of the reported LCST of 32 °C for the PNIPAM homopolymer.[13,14,26,27] Two main factors cause the shift in LCST, namely, the type of ions in the buffer and the incorporation of comonomers in the PNIPAM chain. Lee and co-workers have shown that using 3-(N-morpholino)propanesulfonic acid (MOPS) as a buffer solution can decrease the LCST of the PNIPAM.[26,29] A high dipole moment of zwitterionic buffers such as MOPS or other kosmotropic salt ions produces a condition for stronger affinity toward water molecules and is more prevalent than water−water interactions.[26,29] Such a phenomenon results in a polarization of water molecules that are attached to the amide groups, thus hydrating the PNIPAM.[26] Although MOPS was used in dissolving our copolymers and therefore would lower the LCST, the inclusion of MAA and VP into the polymer chain resulted in an overall increase in the LCST which is consistent with previously reported results by Grenier et al.[14] de Oliveira et al. have also shown that PNIPAM chains copolymerized with acrylamide monomers exhibit a decrease in amide−water hydrogen bonding leading to an increase in the LCST.[34] The lack of reproducibility in the DLS measurement in Figure 3b, as indicated by the error bars, is possibly due to the dynamic polymer aggregation in the MOPS buffer.[35,36]

When left unagitated in a solution, the PNIPAM-based copolymer chains have a tendency to aggregate or "tangle" with one another due to interchain hydrophobic interactions as well as acid−base cross-linking between MAA and VP.[14] However, under constant stirring of the solution, the polymer aggregations gradually untangle over time until they reaches an equilibrium. To assess the time-dependent dispersion of polymer aggregations, the polymers were grafted onto a gold electrode by immersing it for 5 min in the polymer solution that was constantly stirred for a certain period of time. After polymer attachment, the electrochemical impedance across the solution−electrode interface was measured. Figures 3c,d show that the impedance decreases over time then reaches a steady state after approximately a month of polymer dispersion. The

D
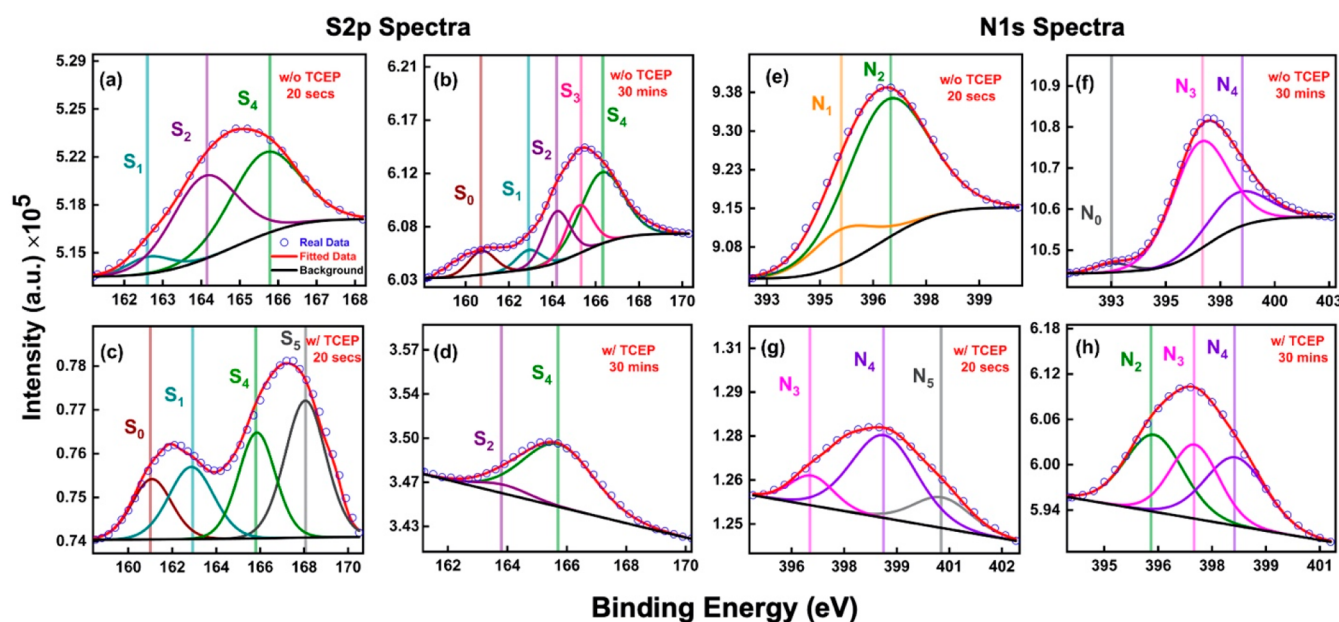
Figure 4. XPS spectra for S 2p (a−d) and N 1s (e−h) of gold electrodes coated with PNIPAM−MAA−VP copolymers with two different grafting times (20 s and 30 min) with and without TCEP. The S 2p spectra analyze the condition of the thiol bond formed at the polymer−gold interface. Legends for the S 2p spectra: S_0: 160.7−161 eV (wine); S_1: 162.6−162.9 eV (dark cyan); S_2: 163.7−164.2 eV (purple); S_3: 165.2 eV (pink); S_4: 165.6−166.2 eV (olive); S_5: 168 eV (dark gray). The N 1s spectra mainly emphasize the functional moieties of PNIPAM and VP. Legends for the N 1s spectra: N_0: 392.5 eV (dark gray); N_1: 395.1 eV (orange); N_2: 395.8−396.4 eV (green); N_3: 396.5−397.5 eV (magenta); N_4: 398.2−398.7 eV (violet); N_5: 400.3 eV (gray). Each figure contains real data (blue hollow circle), fitted data (red curve), and background (black curve). The vertical lines indicate the position of the specific peaks.
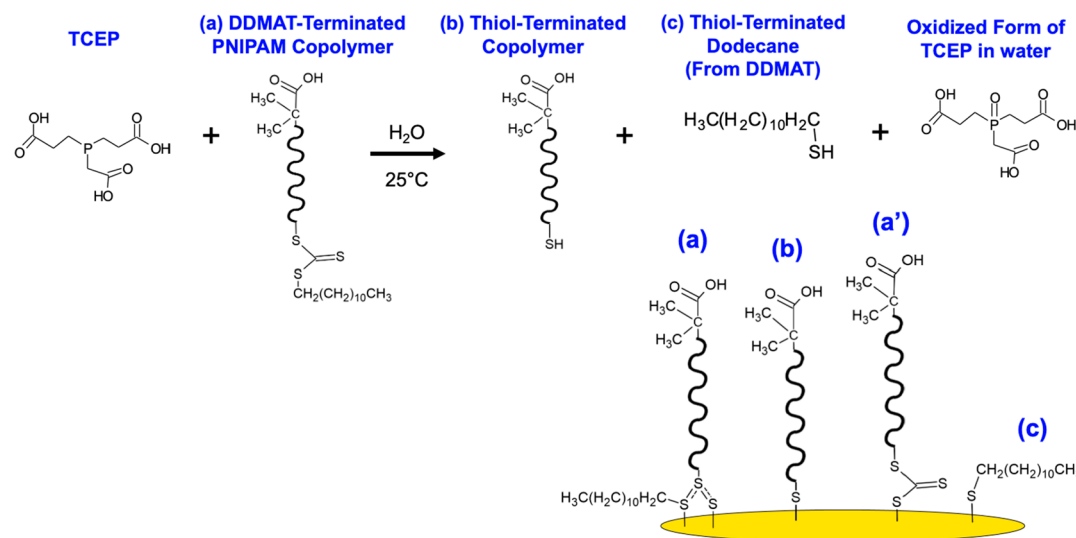
Figure 5. Grafting of the synthesized copolymer chain to a gold electrode. In the presence of TCEP, the DDMAT-terminated copolymer (a) can be converted into a thiol-terminated copolymer (b). Polymers that are grafted to the electrode surface include both DDMAT-terminated (a and a′) and thiol-terminated (b) copolymers. There is also a possible attachment of dodecane groups (c) that have been cleaved from DDMAT assisted by TCEP.

DLS measurement shown in Figure 3a was taken after 1 month (day 32) of dispersion. Therefore, it suggests that after a month of polymer untangling, while most of the polymers are well dispersed, there may still be a small portion of polymer aggregations grafted onto the electrode.

Although DLS was not used for observing binding-induced polymer conformation changes, other optical methods such as fluorescence quenching can be used to confirm this phenomenon.[15] Moreover, similar works have reported a template binding-induced volume change in PNIPAM-based polymers, indicating that the template binding event can act as a stimulus to trigger a polymer shape change.[10,37]

Study of the Surface Chemistry and Grafting of the PNIPAM-Based Copolymers onto Gold Electrode Surface Using XPS. The XPS analysis reveals that as the copolymers are grafted to the gold electrode by converting the trithiocarbonate into a thiol,[38,39] there are several different versions of the covalent cross-linking via the thiol chemistry as indicated by the varying bonding energy. The data also suggest that the polymer grafting time as well as the use of TCEP

(tris(2-carboxyethyl)phosphine) during polymer attachment influences the type of thiol bonding. The XPS measurements were made on PNIPAM-based polymer-attached gold surfaces with two different deposition times (20 s and 30 min) and also with and without the addition of TCEP during polymer grafting. The secure grafting of the polymers on gold was also confirmed by TEM (Supporting Information, section 11).

The core level N 1s and S 2p spectra for the copolymer-modified gold surface are shown in Figure 4 as well as in the Supporting Information (section 2). The spectral analysis indicates that as the polymer grafting time extends (from 20 s to 30 min), the amount of unwanted chemical bonds also increase as evidenced by the prominent N_3 (396.5−397.5 eV), N_4(398.2−398.7 eV), S_4 (165.6−166.2 eV), and S_5 (168 eV) peaks that are prevalent for long deposition times. These peaks correspond to a possible interactions between pyridine and water molecules (N_4)[40] as well as the presence of sulfur oxide complexes (S_4 and S_5) due to the unwanted oxidations that have occurred in the aqueous media.

The absence of TCEP during the grafting of the polymers results in more physisorbed thiols (Table S2), including the disulfide bonding[41] (S_2 peak, 163.7−164.2 eV) as shown in Figure 5 and sulfur oxide (S_4 peak, 165.6−166.2 eV) complexes compared to when TCEP is incorporated, suggesting that TCEP promotes chemisorbed covalent thiol attachment. Cleaning the electrodes with THF after polymer deposition does help remove some but not all traces of physisorbed thiol groups. A longer grafting time without TCEP also results in the adsorption of DDMAT with polymer chain indicated by the peak (S_3 peak, 165.2 eV) due to the (−S−C−S−) bond of DDMAT along with the $CH_3(CH_2)_{10}CH_2$ alkyl chain of the "Z" group.[41−43] The details of the C 1s spectra for the PNIPAM−MAA−VP copolymer-modified gold surface is also discussed in the Supporting Information, section 2.

Because the RAFT chain transfer agent contains three sulfur atoms (trithiocarbonate), upon its reduction, multiple Au−S covalent bonding scenarios can occur between the polymer and the gold surface.[41] When a thiol loses a hydrogen atom to form a gold thiolate, such a proton-subtracted thiolate group $(R−S^-)$ is more chemically reactive than the protonated thiol form $(R−SH)$.[42] Occasionally, a weaker bond can be formed between the protonated SH groups and gold surfaces, resulting in nonspecific binding.[44] Figure 5 describes the reaction for grafting thiol-terminated copolymer chains assisted by TCEP and the possible variations in the thiol bonds between the copolymer and the gold electrode.[30,45] The two different physisorbed thiol terminations (labeled a and a′) are due to trithiocarbonate adsorption onto the gold surface.[30,45,46] The two possible chemisorbed thiol terminations are from the PNIPAM−MAA−VP copolymer grafted to the electrode (labeled b) and from the thiol-terminated dodecane chain from DDMAT (labeled c).[47] In summary, using TCEP during the polymer grafting resulted in a reduced nonspecific attachment of the copolymers while promoting chemisorbed thiol bonding (S_1 peak). However, physisorbed thiol bonds were still prevalent regardless of whether or not TCEP was used during polymer grafting.

Study of Electrode Surface Coverage of the Polymer and Charge Transfer Kinetics of the PNIPAM-Based Copolymer with Varying Grafting Times and Concentrations. The types of anion present in the vicinity of the polymers dispersed in the solution play a greater influence on the stability of our PNIPAM-based target receptors[35,48−50]

than cations do due to the Hofmeister effect.[51,52] The Hofmeister phenomenon, which is prevalent at high anion concentrations,[53] dictates the stability of the polymer−liquid interface by considering the presence of different anions such as chaotropic and kosmotropic ions, which make or break the water structures around the polymer chain.[35,48,50] Chaotropic anions such as NO_3^-, ClO_4^-, SCN^-, and I^- are weakly hydrating and promote direct anion binding to amide moieties ("salting in"), resulting in an increase in the LCST.[35,48,50,54] Moreover, the chaotropic anions stabilize the polymer interface via electrostatic repulsion, dispersion forces, and Coulombic interaction between partially positive regions within the polymer and thus promotes solubility.[50,55] Kosmotropic anions such as CO_3^{2-}, SO_4^{2-}, $H_2PO_4^-$, and Cl^- decrease the water miscibility by polarizing the hydrogen bonding between amide and water molecules, leading to desolvation ("salting out") in the polymer structure and thereby decreasing the LCST (Supporting Information, section 3).[48,54] Therefore, it is critical to take into consideration the effects of anions in the solution when characterizing binding-induced conformation changes of the polymer-based receptors.

All electrochemical measurements were performed at room temperature (~25 °C) which is sufficiently below the LCST of the PNIPAM−MAA−VP copolymer. This operating temperature ensures that the effects of hydrophobic interactions from the isopropyl groups in the PNIPAM backbone are negligible.[14] The 1× PBS containing 0.137 M NaCl, 2.7 mM KCl, and 11.9 mM $H_2PO_4^-$ was used for the experiment. The Cl^- anions from NaCl and KCl salts contribute to the decrease in the LCST by increasing the surface tension via hydrophobic hydration and the weakening of the hydrogen bond between water molecules and amide groups ("salting out"). Moreover, the $H_2PO_4^-$ ions have strong hydrating effects and further contribute to the decrease in the LCST of PNIPAM.[26,48,56] The heterogeneity of the copolymer, namely the inclusion of monomers MAA and VP, has little effect in the polymer's phase transition. Instead, the molar percentage variation of PNIPAM is the primary factor that determines the polymers phase transition.

Electrochemical impedance spectroscopy (EIS) is a suitable method for assessing the kinetics and surface coverage of the polymer−gold interface as well as to effectively analyze the kinetically irreversible polymer layers. The Randle's circuit parameters shown in Figure 5a and Tables S4 and S5 (Supporting Information, section 4) consist of R_s, the uncompensated solution resistance, in series with a parallel combination of a constant phase element (CPE), denoted Q, and the Faradaic impedance (R_{ct} and W).[57] The Faradaic impedance consists of a series combination of a charge transfer resistance (R_{ct}) and the Warburg impedance (W). The dynamic variations in the state of the polymer conformations result in a heterogeneous electrochemical activity modeled via the parallel combination of CPE (Q) and the Faradaic impedance.[17] The Q is attributed to the frequency-dispersive nonideal capacitive behavior of the double-layer capacitance originating from spatial inhomogeneity of the porous PNIPAM copolymer−gold interface.[57,58] The impedance Z_Q due to Q is described by[59]

$$Z_Q = \frac{1}{Q(j\omega)^n} \tag{1}$$

where n ($0 < n < 1$) is the parameter that governs the CPE behavior and ω is the frequency. For a typical Q behavior, n is
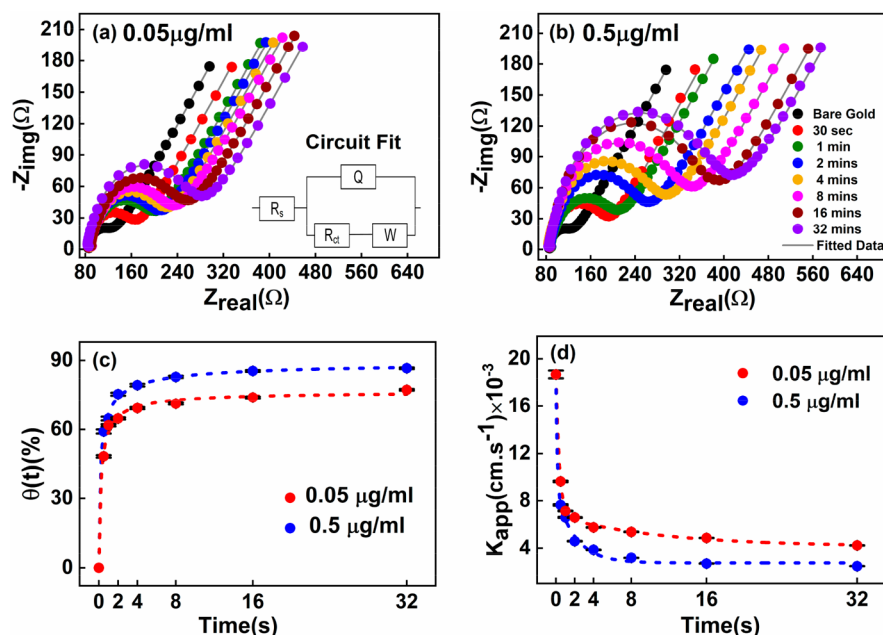
Figure 6. Electrode surface coverage characterization using EIS for two different polymer concentrations, (a) 0.05 μg/mL and (b) 0.5 μg/mL, with varying polymer grafting times. The inset in (a) shows the circuit fit for the Nyquist plots for both polymer concentrations. (c) shows the surface coverage $\theta(t)$ plot for the grafted polymer as a function of time for both polymer concentrations. (d) Change in the apparent rate constant (K_{app}) as a function of time. The time-dependent rate constant profiles follow the two-phase exponential decay model. Legends for (a) and (b): bare gold (black); 30 s (red); 1 min (green); 2 min (blue); 4 min (orange); 8 min (magenta); 16 min (brown); 32 min (violet); fitted data (gray). Legends for (c) and (d): 0.05 μg/mL (red); fitted curve for 0.05 μg/mL (red dotted line); 0.5 μg/mL (blue); fitted curve for 0.5 μg/mL (blue dotted line).

0.5.[60] For n close to one, the Q behaves as a perfect capacitor. If n is close to zero, it changes to a more resistive behavior. The impedance Z_{RQ} due to the nonuniform polymer–gold interface is described as[61]

$$Z_{RQ} = \frac{R_{ct}}{1 + R_{ct}Q(j\omega)^n} \tag{2}$$

The $R_{ct}Q$ suggests that the interfacial pores create abundant openings with heterogeneous charge transfer as Q arises from the highly noncontinuous nature of the interface. Therefore, diffusion of electroactive species can occur via multiple pores. At high frequency ($1 \ll R_{ct}Q(j\omega)^n$), the impedance of the porous interface behaves like a frequency dispersive version of capacitance or CPE.[62] This suggests that the high frequency AC signal is unable to penetrate deep into the porous polymer layer due to the *IR* drop and therefore results in a low porous interface impedance. At low frequencies ($1 \gg R_{ct}Q(j\omega)^n$), the AC signal can penetrate much deeper compared to the high-frequency case and thus results in a resistive impedance. The Warburg impedance (Z_w) is due to mass transfer via pores assuming a semi-infinite diffusion process and is dependent on the concentration of the electroactive species. The Z_w is given by[63]

$$Z_w = \frac{1}{Y_w\sqrt{j\omega}} \tag{3}$$

where Y_w is the admittance of diffusion and ω is the frequency. The circuit fitting provides the Warburg coefficient (A_w) with a semi-infinite diffusion model. Such diffusion suggests highly oriented and uniformly distributed polymer chain depositions on the electrode with minimum interchain interactions.[64]

The reproducibility of the polymer attachment to the electrode surface was confirmed via *t* tests. The two-tailed *t* test

performed on Warburg coefficient (A_w) values ($n = 3$) were at a 95% confidence interval ($p < 0.05$) for two different deposition times and two different concentration values. The *t* test results also indicate that, irrespective of the deposition time and polymer concentrations, the polymer arrangements at the electrode surface are consistent, namely uniformly distributed and highly oriented. The one-way ANOVA test was performed ($n = 3$) with significance defined as $p < 0.05$ to check whether the device-to-device surface variation was significant. The error value was within ± 10.18% (standard error of the mean), indicating relatively minor variations.[65]

The surface coverage achieved by the copolymer can be estimated by the equation[57]

$$\theta(t) = \left[1 - \left(\frac{R_{ct,\text{bare gold}(t=0)}}{R_{ct,\text{polymer}(t)}}\right)\right] \times 100 \tag{4}$$

For 0.05 μg/mL polymer concentration, 61−64% polymer coverage was achieved for the grafting time of 1−2 min (Table S6). For the same grafting time, 64−75% of polymer coverage was achieved for 0.5 μg/mL polymer concentration (Table S7). The surface coverage over different polymer grafting time follows the Langmuir−Freundlich (LF) isotherm:[66]

$$\theta(t) = \frac{\theta_{sat}kt^n}{1 + (kt^n)} \tag{5}$$

The saturation percentage θ_{sat} estimates the majority fraction of the polymer chains attached to the gold surface, which in turn influences the charge transfer during the capacitive buildup. Under two different concentrations of the polymer (0.05 and 0.5 μg/mL), the variation in θ_{sat} was within 13% for the range of grafting time conducted (Table S8 and Figure 6), which demonstrates that the LF isotherm model is consistent
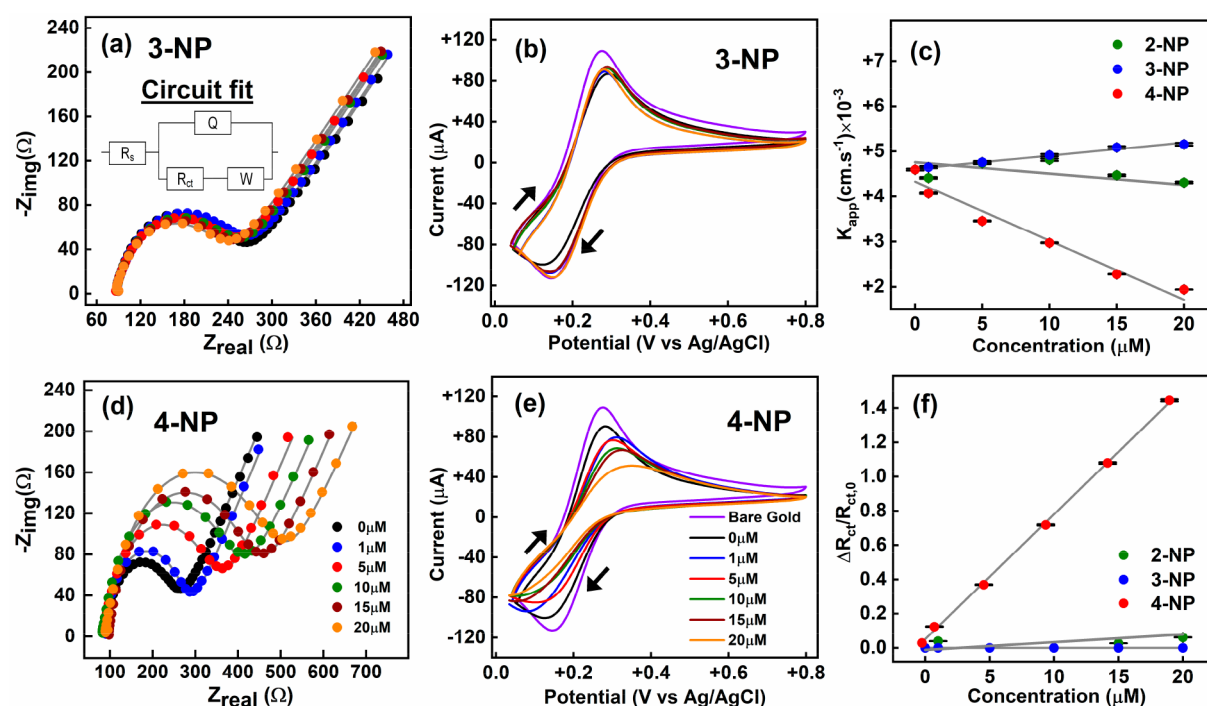
Figure 7. Target binding characterization for the electrochemical sensing of 4-NP. The Nyquist plots after exposing the polymer-modified electrode to varying concentrations of 3-NP (a, b) and 4-NP (d, e). The binding of the template (4-NP) results in a change in the charge transfer kinetics at the polymer−gold interface. The plots in (b) and (e) show the changes in the cyclic voltammetry (CV) when exposed to 3-NP and 4-NP, respectively. The plot in (c) shows the difference in the apparent rate constant (K_{app}) upon specific binding of 4-NP (red) compared to 3-NP (blue) and 2-NP (green). The plot in (f) shows the change in the charge transfer resistance ($\Delta R_{ct}/R_{ct,0}$) of the templated polymer versus target (4-NP) concentration. In the case of 3-NP and 2-NP, the R_{ct} change and K_{app} do not show any significant trend as a function of concentration. For each experiment, the nitrophenol sample (2-, 3-, or 4-NP) was exposed for 1 min to the electrode prior to electrochemical measurements. Legends for (a, b, d, e): 0 μM (black); 1 μM (blue); 5 μM (red); 10 μM (green); 15 μM (brown); 20 μM (orange). The arrows in (b) and (e) represent forward and reverse directions of CV.

throughout various grafting conditions. Having the heterogeneity index equal to one ($n = 1$) reduces the LF model to the Langmuir isotherm, which resembles a homogeneous and uniform distribution of polymer chains at the interface. When $n = 0$, it models a highly heterogeneous and nonuniform distribution of the polymer layer and thus transforms the model to Freundlich isotherm.[66] Our PNIPAM copolymer deposition on the gold surface exhibited both homogeneous and heterogeneous distributions for both high and low polymer concentrations. For 0.05 μg/mL polymer concentration, the heterogeneity index of $n = 0.8$ was obtained which signified more homogeneous deposition of the polymers with less interchain cross-linking compared to the 0.5 μg/mL polymer concentration which had the heterogeneity index of $n = 0.6$. The median grafting density increases approximately 1.4-fold in response to a 10-fold increase in the polymer concentration.

The apparent rate constant (K_{app}) determines the rate of charge transfer via redox reaction at the polymer−gold interface. The K_{app} was calculated via the following equation:[67]

$$K_{app} = \frac{RT}{nF^2 C A R_{ct}} \tag{6}$$

The results suggest that heterogeneous diffusion of electro-active species and the variability of the diffusion depth are the primary rate-determining factors that govern the kinetics in PNIPAM copolymer-modified gold electrode. K_{app} decays as the polymer deposition progresses, and it exhibits two distinct kinetics: one is related to the uniformly deposited minimally

cross-linked polymer, and the other is the nonuniform highly cross-linked polymer. The decay in K_{app} indicates the increase in the average grafting density of polymer chains at the gold surface. The initial decline of K_{app} in Figure 6d is attributed to the formation of clusters due to the coalescence of hydrated or cross-linked polymer chains. The parameter fitting (Supporting Information, section 5) of the time-dependent K_{app} reveals the presence of two different time constants τ_1 and τ_2 (Table S9): τ_1, a shorter time constant, is due to the steady diffusion path for the uniformly distributed and minimally cross-linked polymer chains; τ_2, a longer time constant, is due to the deposition of nonuniform highly cross-linked polymer chains. The longer time constant (τ_2) may have been influenced by the salting-out effect, indicating the presence of a highly disordered polymer entanglement at the interface.

Electrochemical Impedance Spectra of 4-NP-Templated PNIPAM Copolymer Shows a Selective Change in Charge Transfer Resistance and Kinetics. To assess the feasibility of the synthesized templated polymer as a target receptor for the electrochemical sensing platform, the polymer-grafted electrode was exposed to 4-nitrophenol (4-NP) for a fixed amount of time (1 min) to evaluate its sensing performances. The 4-NP-templated single-chain PNIPAM copolymerized with MAA and VP was grafted onto the electrode with 0.5 μg/mL polymer concentration to attain ∼75% surface coverage. Despite the heterogeneous nature of polymer grafting influenced by aggregation, a nonuniform distribution of the grafted polymers, and the acid−base noncovalent inter- and intrachain cross-linking,[14] a significant

portion of the polymers were highly oriented with minimum interchain cross-linking. These polymer-based target receptors that are grafted on the electrode undergo distinct conformational changes upon target binding. Such conformational change of the templated polymer results in a distinguishable change in the electrochemical signals via altering the interface charge transfer kinetics (Supporting Information, section 6). A measurable difference in the charge transfer resistance (R_{ct}) is observed as 4-NP molecules are bound to the PNIPAM-based copolymers, impeding the diffusion of the electroactive species. The selectivity of the receptors was assessed by exposing the sensor to the target's isomers: 2-nitrophenol (2-NP) and 3-nitrophenol (3-NP). The 4-NP-templated polymer-modified electrode does not go through any visible or quantifiable change in R_{ct} during exposure to 2-NP and 3-NP (Figure 7, Table S12, and Figure S8). The changes associated with R_{ct} in the case of 3-NP can be attributed primarily to the hydrogen bonding with the functional monomers in PNIPAM. The receptor's target affinity was estimated by measuring the change in charge transfer resistance $\frac{\Delta R_{ct}}{R_{ct,0}}$ via the equation[68]

$$\frac{\Delta R_{ct}}{R_{ct,0}} = \left| \frac{R_{ct} - R_{ct,0}}{R_{ct,0}} \right|_{n>0} \qquad (7)$$

Upon target binding, the polymer's conformational change results in a higher R_{ct} as well as enhanced interface capacitance. There may be a small percentage of the polymers on the electrode that do not have functioning binding sites and thus do not exhibit conformational changes even in the presence of the target molecules. The variation in the proportion of such nonfunctional polymer chains may result in a constant value of the diffusion resistance, thus affecting the A_w values at low frequency.[68,69] The polymer chains that either have no binding sites or do not bind due to partial hydration caused by kosmotropic anion interaction also contribute to changes in A_w values. Upon comparison of the results between exposure to 4-NP and 3-NP, the R_{ct} values for 0 μM have no significant differences. However, the value of the Warburg coefficient (A_w) corresponding to 3-NP is higher than that of 4-NP. Such difference may come from the impediment in diffusion due to the discontinuous and nonuniform clustering of polymer chains triggered via cooperative dehydration of the polymer chains experiencing kosmotropic effects (Tables S10 and S11).[70] The K_{app} was calculated for each concentration of the target 2-NP, 3-NP, and 4-NP (Figure 7c and Table S12). In Figure 7c, the concentration-dependent changes in K_{app} are observed (particularly for 4-NP) where a decrease in K_{app} is indicative of an increase in the target affinity due to an increase in R_{ct} caused by the polymer's conformation change. The slope for the 4-NP plot is found to be $(-0.13 \pm 0.01) \times 10^{-3}$ cm s^{-1} μM^{-1} with $R^2 = 0.9818$. This slope value indicates a significant disruption in the normal charge transfer kinetics upon specific target binding. By comparison, the 3-NP plot has the slope of $(0.02 \pm 0.002) \times 10^{-3}$ cm s^{-1} μM^{-1} with $R^2 = 0.99369$, depicting only a negligible increase in the charge transfer kinetics. The 2-NP slope of $(0.005 \pm 0.004) \times 10^{-3}$ cm s^{-1} μM^{-1} with $R^2 = 0.96553$ also shows no significant change in the kinetics. An ~6.5-fold increase in absolute slope value for 4-NP compared to the other 2 species indicates a substantial disruption of charge transfer kinetics upon specific 4-NP binding. Figure 7c also shows a minuscule increase in the slope for 2-NP and 3-NP which may be attributable to nonspecific

hydrogen bonding between MAA and the isomers of 4-NP. The slope of the plot of K_{app} for 4-NP shows a significant negative trend which signifies increased capacitive contribution at the interface upon target recognition. With regard to concentration-dependent R_{ct} changes, the curve-fitting model suggests that the template affinity $\left(\frac{\Delta R_{ct}}{R_{ct,0}} \right)$ vs 4-NP concentration plot follows a linearized Langmuir isotherm model,[68] unlike the plots for 3-NP and 2-NP concentrations which had no significant changes as shown in Figure 7f, Figure S8, and Table S12. No significant 2-NP and 3-NP affinities suggest a highly selective nature of the templated polymer-based 4-NP receptor. The CV plots in Figure 7b,e depict a rapid change in the kinetics, indicating reaction irreversibility resulting in the hindered charge transfer at the interface due to the polymer conformational changes. During CV measurements, the potential sweep can alter the polymer chain conformation at the interface and thus can introduce variation in the diffusion of the charged species from bulk to the depletion layer, which may further add to the irreversibility of the CV. To further confirm the specificity of the templated polymer-based receptor, it was compared against a nontemplated copolymer synthesized under the same conditions but in the absence of the template. The nontemplated PNIPAM–MAA–VP copolymers exhibited no significant binding upon exposure to the 4-NP, suggesting the effectiveness of molecular templating (Figures S15 and S16).[14]

To assess the reliability of our detection platform, the developed senor was tested under real water samples collected from the local river. A similar test was also performed with a laboratory tap water (Supporting Information, section 9). Moreover, to further characterize the sensor's selectivity against interfering species, three organic compounds—phenol, 2-chlorophenol, and 2-aminophenol (each having the same concentration ranging from 0 to 20 μM)—were added to the sample water. As shown in Figure 8, the collected river water initially had no measurable traces of 4-NP, and the sensor's response was minimally affected by the interferents. When a known concentration of 4-NP was added to the water sample, the R_{ct} change ($\Delta R_{ct}/R_{ct,0}$) followed a linear response with respect to the 4-NP concentration. This demonstrates the sensor's chemical selectivity and its ability to detect 4-NP from real water samples. The reproducibility and stability of the developed sensor were also verified (Supporting Information, section 10).

■ CONCLUSION

In this work, we have demonstrated a new electrochemical sensing platform by implementing a single-chain templated PNIPAM-based copolymer as a novel target receptor. Upon specific target recognition, the polymer receptor undergoes conformation change from an extended wirelike state to a folded shape. The DLS measurements show that the presence of kosmotropic anions strongly influence the hydrodynamic behavior and colloidal stability of the polymer leading to dynamic aggregation under LCST. The addition of TCEP improves the polymer's chemisorption to the electrode by reducing the RAFT agent to the thiol group. A longer grafting time leads to an increase in unwanted physisorbed polymers at the electrode while a shorter grafting time increases the probability of obtaining well-oriented chemisorbed polymer chains. With such highly uniform polymer arrangement, the
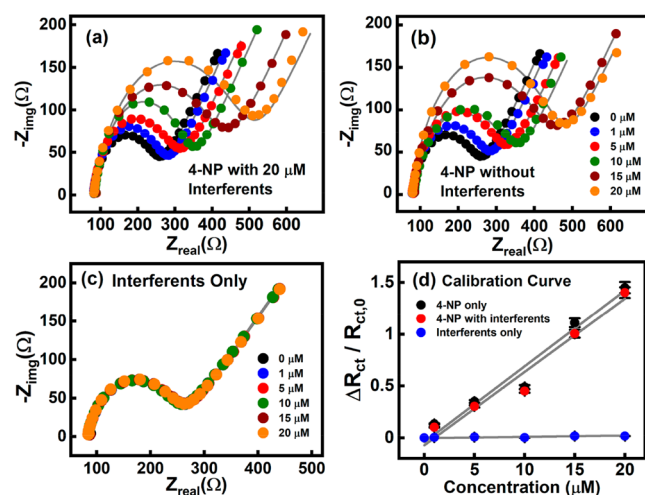
Figure 8. Selective binding of 4-NP assessed via electrochemical sensing on the river water. (a) The Nyquist plot for the sensor when exposed to varying concentrations of 4-NP in the presence of a mixture of interferents (20 μM each for phenol, 2-chlorophenol, and 2-aminophenol). (b) Nyquist plot for varying concentrations of 4-NP without any interferents added. (c) Nyquist plot for varying concentrations of interferents (same concentration for all three species). (d) Calibration curve showing the change in the charge transfer resistance ($\Delta R_{ct}/R_{ct,0}$) vs 4-NP concentrations. Legends for (a−c): 0 μM (black); 1 μM (blue); 5 μM (red); 10 μM (green); 15 μM (brown); 20 μM (orange). Legends for (d): 4-NP only (black), 4-NP with interferents (red), and interferents only (blue).

target-induced folding of the polymers impedes the diffusion of electroactive species at the polymer−electrode interface. A linear trend with a negative slope in the apparent rate constant signifies a substantial decrease in the charge transfer rate as more target species are bound to the receptors. The sensor was selective to 4-NP even in the presence of interfering species and isomer variants in tap and river water samples. The proposed sensing approach can potentially be expanded into a general platform technology for detecting a variety of chemical species through the use of a conformation changing single-chain templated copolymers.

■ MATERIALS AND METHODS

Material Preparation and Purification of Chemicals. Methacrylic acid (MAA) and 4-vinylpyridine (VP) were both purchased from Sigma-Aldrich (St. Louis, MO). Prior to usage, MAA and VP were first vacuum distilled and then were passed through columns of basic alumina and inhibitor removers. *N*-Isopropylacrylamide (NIPAM) at 99% purity from TCI (Portland, OR) was recrystallized from hexane multiple times for removing the inhibitors before use. In addition, 2,2′-azobis(isobutyronitrile) (AIBN), inhibitor removal beads, 1,4-dioxane (99.8% anhydrous), methanol (ACS grade), hexane (ACS grade), and 2-(dodecylthio-carbonothioylthio)2-methylpropanoic acid (DDMAT, 97%) were obtained from Sigma-Aldrich and were used as received. All other chemicals were purchased from Sigma-Aldrich unless otherwise specified. The dialysis membranes (Spectrapor 2) were obtained from Cole-Parmer.

Polymer Synthesis via Reversible Addition−Fragmentation Chain Transfer (RAFT) Process. All polymers were synthesized via the RAFT process formulated by the Seitz group. The overall polymerization process is based on the method previously reported in Grenier et al. with minor modifications as described below.[14,15,17,18] The synthesis of the PNIPAM homopolymer involves dissolving purified NIPAM (2.825 g, 25 mmol), DDMAT (chain transfer agent, 0.091 g, 0.25 mmol), and AIBN (initiator, 0.008 g, 0.05 mmol) in 25

mL of 1,4-dioxane using a 50 mL round-bottom flask with a magnetic stir bar. Afterward, the flask was sealed with a rubber septum. Then the mixture was degassed by a freeze−pump−thaw technique three times followed by backfilling with nitrogen. The flask was heated at 70 °C while stirring in an oil bath for 24 h. The synthesis of the nitrophenol-templated PNIPAM−MAA−VP copolymers was performed by dissolving 4-NP (template molecule, 26 mg, 0.25 mmol), NIPAM (2.150 g, 19 mmol), MAA (0.212 μL, 2.5 mmol), VP (0.377 μL, 3.5 mmol), DDMAT (0.091 g, 0.25 mmol), and AIBN (0.008 g, 0.05 mmol) in 25 mL of 1,4-dioxane. The molar ratio between the monomers and the template (4-NP) was fixed to 100:1. The remaining polymerization steps were identical with that of the PNIPAM homopolymers.

After polymerization, the unreacted monomers and the template molecules were separated from the polymers via dialysis. Approximately 20 mL of the solution containing the polymers was aliquoted into the dialysis tubing with a 10000−12000 molecular weight cut off (MWCO) dialysis membrane. The dialysis process consisted of two steps. In the first step, the polymer solution was dialyzed against 700 mL of 50% (v/v) THF in a beaker with magnetic stirring at room temperature. The dialysis solvent was replaced with a fresh THF every 8−24 h period. This step continued for 2−6 weeks. In the second step, the solution was dialyzed against 0.1 M NaOH in 30% (v/v) methanol and 5% (v/v) acetic acid solution at 60 °C. This template removal process ran for another 3 weeks. After the template removal, the polymer solution was dialyzed against DI water three times followed by lyophilization. The polymers were freeze-dried with the Labconco Freezone 2.5 Lite benchtop freeze-dry system. The freeze-dry system was used to remove water from the polymer, yielding a powder formation. The pressure was kept near 0.130 Torr with the temperature brought down to −80 °C, below water's triple point. Such a freeze-dryer initiates the expulsion of water through sublimation, resulting in a template-free grayish powder of PNIPAM−MAA−VP copolymer sample.

Sample Preparation for FTIR and DLS Measurements of PNIPAM−MAA−VP Polymers. The FTIR measurements were performed in the Thermo Nicolet iS10 FT-IR with a resolution of 0.4 cm^{-1} and a dynamic spectral range from 7800 to 350 cm^{-1}. The data analysis was performed on the OMNIC-8 software. The lyophilized polymer powders were directly subjected to measurements through a diamond attenuated total reflectance (ATR) unit integrated with the FTIR instrument. Before each analysis, the ATR surface was cleaned via ethanol to minimize the effect of impurities. The DLS measurements were performed on a Malvern Zetasizer Nano NS by dissolving 10 mg of the polymer powder dissolved in 10 mL of MOPS buffer having pH 7.0 in a quartz cuvette. Before DLS measurements, the polymer powder was dissolved for more than 30 days while maintaining the same pH level to ensure minimally tangled polymer chains, resulting in reproducible DLS measurements. The DLS data acquisition was conducted with Zetsizer software 7.13. For LCST determination, three data points were acquired for each temperature ranging from 15 to 65 °C with increments of 1 °C.

Grafting of the Polymers to a Gold Electrode. After lyophilization, the powder form of PNIPAM-based copolymer samples was dissolved at given concentrations (0.05 and 0.5 μg/mL) in DI water. This solution was kept for at least 3 weeks under continuous stirring with a magnetic stir bar in a sealed container. This procedure was employed to ensure that the powder is fully dissolved and that the polymers are well-dispersed with minimum tangling. The grafting of the copolymers to the gold electrode from the two specified solution concentrations mentioned above was performed by using BASI MF-2114 planar gold (Au) electrodes having a diameter of 3 mm. Prior to the polymer attachment, the electrodes were fully dried via N$_2$ purging. The polymer grafting was realized by exposing the dry electrode to a polymer solution (Figures S9 and S14). During the polymer deposition, TCEP (tris(2-carboxyethyl)phosphine), a reducing agent, was mixed at a 1:1 mass ratio in the depositing solution. The solution was kept under continuous and slow stirring during deposition to achieve a homogeneous distribution of polymers on the electrode surface. After polymer immobilization, the electrode

surface was consecutively rinsed with 50% THF and DI water for 2 min each to remove any nonspecific attachments. Before using the polymer-modified gold electrodes for electrochemical studies, we dried each electrode again via gentle N_2 purging.

Sample Preparation for XPS Measurements on Polymer-Modified Gold Surfaces. For XPS measurements, the PNIPAM–MAA–VP copolymers were grafted to a gold layer which was thermally evaporated on a glass slide. The effective surface area of the gold film was similar to that of the BASI MF-2114 planar gold electrode. A thermal evaporator (Edwards E306A) was used to coat a 60 nm thick gold layer on top of a 5 nm chromium layer. Photolithography was used to pattern the gold surface to adjust the surface area. The polymers were deposited by drop-casting a polymer solution (0.5 μg/mL) under two different deposition times (20 s and 30 min) as well as with and without TCEP. The XPS studies were performed by using a Kratos Axis Supra system with a base pressure of 10^{-9} Torr using the Al Kα (1486.8 eV) X-ray monochromatized radiation with a pass energy of 50 eV (resolution: 0.5 eV). Spectra were taken by averaging the measurements from four different spots of ~15 μm for each sample. The XPS peak fitting was performed by using the ESCApe data acquisition system. All analyses of XPS spectra for polymer samples were compared to the respective baseline spectra of the bare gold surface (Supporting Information, section 2). The binding energy has an estimated error within $\pm$0.8 eV.

Electrochemical Characterization of the Templated Polymer-Modified Gold Electrode. Cyclic voltammetry (CV) and electrochemical impedance spectroscopy (EIS) were performed by using a BioLogic VSP potentiostat in a three-electrode setup in a small-volume cell (BioLogic, SVC 3) having a platinum coil (BioLogic: A-002234) as a counter electrode. The Ag/AgCl electrode (BioLogic: RE-1B) was used as a reference. The electrolyte used in the experiment consists of 5 mM $K_{4/3}Fe(CN)_6$ dissolved in 1$\times$ PBS with pH 7.1. The electrolyte was prepared fresh for each experiment and purged with N_2. The CV was performed at a scan rate of 100 mV s^{-1} from 0.0 to +0.85 V, with a step voltage of 10 mV. The EIS measurements were taken with a frequency range from 0.1 Hz to 100 kHz with the bias kept at open circuit potential (OCP). The bias was kept in OCP to ensure proper redox activity of equimolar electroactive species at the polymer–gold interface. The maximum frequency of 100 kHz was selected to minimize the inductance effect. The EIS circuit fit was performed via a complex nonlinear least-squares (CNLS) method in EC-Lab software to interpret the physical interface model, including cross-linking and aggregation.[69] For CV and EIS, the measurements were repeated three times (n = 3). For electrode preparation, the polymers were grafted onto the electrode for 2 min by using a polymer solution with a concentration of 0.5 μg/mL. For analyte sensing (4-NP) and selectivity characterization (2-NP and 3-NP), the polymer-grafted electrode was exposed to 20 mL of a sample solution containing the nitrophenol species with concentrations ranging from 0 to 20 μM for 1 min. Origin Pro software (ver. 2019b) was used for the statistical calculations as well as graphical presentation of the experimental data.

■ ASSOCIATED CONTENT

Ⓢ Supporting Information

The Supporting Information is available free of charge at https://pubs.acs.org/doi/10.1021/acsapm.0c01120.

> Additional details about the method, material characterization, and electrochemical studies (PDF)

■ AUTHOR INFORMATION

Corresponding Author

Edward Song − *Department of Electrical and Computer Engineering and Materials Science Program, University of New Hampshire, Durham, New Hampshire 03824, United States;* ⓘ orcid.org/0000-0003-1702-4044; Phone: +1-603-862-5498; Email: Edward.Song@unh.edu

Authors

Habib M. N. Ahmad − *Department of Electrical and Computer Engineering, University of New Hampshire, Durham, New Hampshire 03824, United States*

Gaurab Dutta − *Department of Electrical and Computer Engineering, University of New Hampshire, Durham, New Hampshire 03824, United States*

John Csoros − *Department of Chemistry, University of New Hampshire, Durham, New Hampshire 03824, United States*

Bo Si − *Department of Chemistry, University of New Hampshire, Durham, New Hampshire 03824, United States*

Rongfang Yang − *Department of Chemistry, University of New Hampshire, Durham, New Hampshire 03824, United States*

Jeffrey M. Halpern − *Department of Chemical Engineering, University of New Hampshire, Durham, New Hampshire 03824, United States;* ⓘ orcid.org/0000-0003-0814-1986

W. Rudolf Seitz − *Department of Chemistry, University of New Hampshire, Durham, New Hampshire 03824, United States;* ⓘ orcid.org/0000-0002-9128-0145

Complete contact information is available at:
https://pubs.acs.org/10.1021/acsapm.0c01120

Author Contributions

Habib M.N. Ahmad and Gaurab Dutta contributed equally.

Notes

The authors declare no competing financial interest.

■ ACKNOWLEDGMENTS

■ REFERENCES

(1) Poma, A.; Turner, A. P. F.; Piletsky, S. A. Advances in the Manufacture of MIP Nanoparticles. *Trends Biotechnol.* **2010**, *28* (12), 629−637.

(2) Ye, L.; Mosbach, K. Molecular Imprinting: Synthetic Materials As Substitutes for Biological Antibodies and Receptors. *Chem. Mater.* **2008**, *20* (3), 859−868.

(3) Chen, L.; Wang, X.; Lu, W.; Wu, X.; Li, J. Molecular Imprinting: Perspectives and Applications. *Chem. Soc. Rev.* **2016**, *45* (8), 2137−2211.

(4) Chen, L.; Xu, S.; Li, J. Recent Advances in Molecular Imprinting Technology: Current Status, Challenges and Highlighted Applications. *Chem. Soc. Rev.* **2011**, *40* (5), 2922−2942.

(5) Gorska, K.; Huang, K.-T.; Chaloin, O.; Winssinger, N. DNA-Templated Homo- and Heterodimerization of Peptide Nucleic Acid Encoded Oligosaccharides That Mimick the Carbohydrate Epitope of HIV. *Angew. Chem., Int. Ed.* **2009**, *48* (41), 7695−7700.

(6) Rachkov, A.; Minoura, N. Towards Molecularly Imprinted Polymers Selective to Peptides and Proteins. The Epitope Approach. *Biochim. Biophys. Acta, Protein Struct. Mol. Enzymol.* **2001**, *1544* (1), 255−266.

(7) Saylan, Y.; Yilmaz, F.; Özgür, E.; Derazshamshir, A.; Yavuz, H.; Denizli, A. Molecular Imprinting of Macromolecules for Sensor Applications. *Sensors* **2017**, *17* (4), 898.

(8) Hillberg, A. L.; Brain, K. R.; Allender, C. J. Molecular Imprinted Polymer Sensors: Implications for Therapeutics. *Adv. Drug Delivery Rev.* **2005**, *57* (12), 1875−1889.

(9) Guo, X.; Li, J.; Arabi, M.; Wang, X.; Wang, Y.; Chen, L. Molecular-Imprinting-Based Surface-Enhanced Raman Scattering Sensors. *ACS Sens.* **2020**, *5* (3), 601−619.

(10) Watanabe, M.; Akahoshi, T.; Tabata, Y.; Nakayama, D. Molecular Specific Swelling Change of Hydrogels in Accordance with the Concentration of Guest Molecules. *J. Am. Chem. Soc.* **1998**, *120* (22), 5577−5578.

(11) Sahn, M.; Yildirim, T.; Dirauf, M.; Weber, C.; Sungur, P.; Hoeppener, S.; Schubert, U. S. LCST Behavior of Symmetrical PNiPAm-b-PEtOx-b-PNiPAm Triblock Copolymers. *Macromolecules* **2016**, *49* (19), 7257−7267.

(12) Futscher, M. H.; Philipp, M.; Müller-Buschbaum, P.; Schulte, A. The Role of Backbone Hydration of Poly(N-Isopropyl Acrylamide) Across the Volume Phase Transition Compared to Its Monomer. *Sci. Rep.* **2017**, *7* (1), 1−10.

(13) Ono, Y.; Shikata, T. Hydration and Dynamic Behavior of Poly(N-Isopropylacrylamide)s in Aqueous Solution: A Sharp Phase Transition at the Lower Critical Solution Temperature. *J. Am. Chem. Soc.* **2006**, *128* (31), 10030−10031.

(14) Grenier, C. J.; Timberman, A.; Yang, R.; Csoros, J.; Papantones, A.; Deravi, L. F.; Seitz, W. R. Rapid, High Affinity Binding by a Fluorescein Templated Copolymer Combining Covalent, Hydrophobic, and Acid-Base Noncovalent Crosslinks. *Sensors* **2018**, *18* (5), 1330.

(15) Yang, R. *Development of Fluorescent Sensors Based on Molecularly Imprinted Biomimetic Polymers*; University of New Hampshire, 2018.

(16) Xiao, Y.; Lubin, A. A.; Heeger, A. J.; Plaxco, K. W. Label-Free Electronic Detection of Thrombin in Blood Serum by Using an Aptamer-Based Sensor. *Angew. Chem., Int. Ed.* **2005**, *44* (34), 5456−5459.

(17) Ahmad, H. M. N.; Si, B.; Dutta, G.; Csoros, J. R.; Seitz, W. R.; Song, E. Non-Enzymatic Electrochemical Detection Of Glutamate Using Templated Polymer-Based Target Receptors. *In 2019 20th International Conference on Solid-State Sensors, Actuators and Microsystems Eurosensors XXXIII (Transducers/Eurosensors XXXIII)* **2019**, 613−616.

(18) Dutta, G.; Yang, R.; Ahmad, H. M. N.; Si, B.; Csoros, J.; Ren, T.; Halpem, J. M.; Rudolf Seitz, W.; Song, E. A Single-Chain Templated Polymer-Based Target Receptor as a New Platform for Label-Free Selective Electrochemical Sensing. *In 2019 41st Annual International Conference of the IEEE Engineering in Medicine and Biology Society (EMBC)* **2019**, 1163−1166.

(19) Li, J.; Kuang, D.; Feng, Y.; Zhang, F.; Xu, Z.; Liu, M. A Graphene Oxide-Based Electrochemical Sensor for Sensitive Determination of 4-Nitrophenol. *J. Hazard. Mater.* **2012**, *201−202*, 250−259.

(20) Hryhorczuk, D. O.; Moomey, M.; Burton, A.; Runkle, K.; Chen, E.; Saxer, T.; Slightom, J.; Dimos, J.; McCann, K.; Barr, D. Urinary P-Nitrophenol as a Biomarker of Household Exposure to Methyl Parathion. *Environ. Health Perspect.* **2002**, *110* (6), 1041−1046.

(21) Masqué, N.; Marcé, R. M.; Borrull, F.; Cormack, P. A. G.; Sherrington, D. C. Synthesis and Evaluation of a Molecularly Imprinted Polymer for Selective On-Line Solid-Phase Extraction of 4-Nitrophenol from Environmental Water. *Anal. Chem.* **2000**, *72* (17), 4122−4126.

(22) Caro, E.; Masqué, N.; Marcé, R. M.; Borrull, F.; Cormack, P. A. G.; Sherrington, D. C. Non-Covalent and Semi-Covalent Molecularly Imprinted Polymers for Selective on-Line Solid-Phase Extraction of 4-Nitrophenol from Water Samples. *J. Chromatogr. A* **2002**, *963* (1), 169−178.

(23) Moad, G. RAFT Polymerization to Form Stimuli-Responsive Polymers. *Polym. Chem.* **2017**, *8* (1), 177−219.

(24) Moad, G.; Rizzardo, E.; Thang, S. H. Living Radical Polymerization by the RAFT Process. *Aust. J. Chem.* **2005**, *58* (6), 379−410.

(25) Xu, W.; Yin, X.; He, G.; Zhao, J.; Wang, H. Photografted Temperature-Sensitive Poly(N-Isopropylacrylamide) Thin Film with a Superfast Response Rate and an Interesting Transparent-Opaque-Transparent Change in Its Deswelling Process. *Soft Matter* **2012**, *8* (11), 3105−3111.

(26) Taha, M.; Gupta, B. S.; Khoiroh, I.; Lee, M.-J. Interactions of Biological Buffers with Macromolecules: The Ubiquitous "Smart" Polymer PNIPAM and the Biological Buffers MES, MOPS, and MOPSO. *Macromolecules* **2011**, *44* (21), 8575−8589.

(27) Sun, S.; Hu, J.; Tang, H.; Wu, P. Chain Collapse and Revival Thermodynamics of Poly(N-Isopropylacrylamide) Hydrogel. *J. Phys. Chem. B* **2010**, *114* (30), 9761−9770.

(28) Lang, X.; Lenart, W. R.; Sun, J. E. P.; Hammouda, B.; Hore, M. J. A. Interaction and Conformation of Aqueous Poly(N-Isopropylacrylamide) (PNIPAM) Star Polymers below the LCST. *Macromolecules* **2017**, *50* (5), 2145−2154.

(29) Taha, M.; Lee, M.-J. Solubility and Phase Separation of 4-Morpholinepropanesulfonic Acid (MOPS), and 3-Morpholino-2-Hydroxypropanesulfonic Acid (MOPSO) in Aqueous 1,4-Dioxane and Ethanol Solutions. *J. Chem. Thermodyn.* **2011**, *43* (11), 1723−1730.

(30) Honold, T.; Skrybeck, D.; Wagner, K. G.; Karg, M. Fully Reversible Quantitative Phase Transfer of Gold Nanoparticles Using Bifunctional PNIPAM Ligands. *Langmuir* **2017**, *33* (1), 253−261.

(31) Patterson, J. P.; Kelley, E. G.; Murphy, R. P.; Moughton, A. O.; Robin, M. P.; Lu, A.; Colombani, O.; Chassenieux, C.; Cheung, D.; Sullivan, M. O.; Epps, T. H.; O'Reilly, R. K. Structural Characterization of Amphiphilic Homopolymer Micelles Using Light Scattering, SANS, and Cryo-TEM. *Macromolecules* **2013**, *46* (15), 6319−6325.

(32) Ren, T.; Roberge, E. J.; Csoros, J. R.; Seitz, W. R.; Balog, E. R. M.; Halpern, J. M. Application of Voltage in Dynamic Light Scattering Particle Size Analysis. *J. Visualized Exp.* **2020**, No. 155, 60257.

(33) Zou, J.; Guan, B.; Liao, X.; Jiang, M.; Tao, F. Dual Reversible Self-Assembly of PNIPAM-Based Amphiphiles Formed by Inclusion Complexation. *Macromolecules* **2009**, *42* (19), 7465−7473.

(34) de Oliveira, T. E.; Mukherji, D.; Kremer, K.; Netz, P. A. Effects of Stereochemistry and Copolymerization on the LCST of PNIPAm. *J. Chem. Phys.* **2017**, *146* (3), 034904.

(35) Zhang, Y.; Furyk, S.; Bergbreiter, D. E.; Cremer, P. S. Specific Ion Effects on the Water Solubility of Macromolecules: PNIPAM and the Hofmeister Series. *J. Am. Chem. Soc.* **2005**, *127* (41), 14505−14510.

(36) Fulton, L. A.; Zhang, P.; Seitz, W. R.; Tsavalas, J. G.; Planalp, R. P. Dynamic Aggregation of Poly-N-Isopropylacrylamide Characterized Using Second-Order Scattering. *Appl. Spectrosc.* **2018**, *72* (9), 1341−1348.

(37) Fan, W.; Seitz, W. R. Swellable Theophylline Selective Microparticles for Sensing Applications. *Analyst* **2007**, *132* (11), 1103.

(38) Willcock, H.; O'Reilly, R. K. End Group Removal and Modification of RAFT Polymers. *Polym. Chem.* **2010**, *1* (2), 149−157.

(39) Burns, J. A.; Butler, J. C.; Moran, J.; Whitesides, G. M. Selective Reduction of Disulfides by Tris(2-Carboxyethyl)Phosphine. *J. Org. Chem.* **1991**, *56* (8), 2648−2650.

(40) Zhai, G. PH- and Temperature-Sensitive Microfiltration Membranes from Blends of Poly(Vinylidene Fluoride)-Graft-Poly(4-Vinylpyridine) and Poly(N-Isopropylacrylamide). *J. Appl. Polym. Sci.* **2006**, *100* (5), 4089−4097.

(41) Jia, J.; Kara, A.; Pasquali, L.; Bendounan, A.; Sirotti, F.; Esaulov, V. A. On Sulfur Core Level Binding Energies in Thiol Self-Assembly and Alternative Adsorption Sites: An Experimental and Theoretical Study. *J. Chem. Phys.* **2015**, *143* (10), 104702.

(42) Poole, L. B. The Basics of Thiols and Cysteines in Redox Biology and Chemistry. *Free Radical Biol. Med.* **2015**, *80*, 148−157.

(43) Zareie, H. M.; Boyer, C.; Bulmus, V.; Nateghi, E.; Davis, T. P. Temperature-Responsive Self-Assembled Monolayers of Oligo-

(Ethylene Glycol): Control of Biomolecular Recognition. *ACS Nano* **2008**, *2* (4), 757−765.

(44) Xue, Y.; Li, X.; Li, H.; Zhang, W. Quantifying Thiol-Gold Interactions towards the Efficient Strength Control. *Nat. Commun.* **2014**, *5* (1), 1−9.

(45) Ebeling, B.; Vana, P. RAFT-Polymers with Single and Multiple Trithiocarbonate Groups as Uniform Gold-Nanoparticle Coatings. *Macromolecules* **2013**, *46* (12), 4862−4871.

(46) Mishra, S.; Rawal, A.; Nebhani, L. Imprinting the Location of an In-Built RAFT Agent and Selective Grafting of Polymer Chains inside or Outside the Pores of Mesoporous Silica Nanoparticles. *Microporous Mesoporous Mater.* **2020**, *294*, 109898.

(47) Zhong, C.-J.; Brush, R. C.; Anderegg, J.; Porter, M. D. Organosulfur Monolayers at Gold Surfaces: Reexamination of the Case for Sulfide Adsorption and Implications to the Formation of Monolayers from Thiols and Disulfides. *Langmuir* **1999**, *15* (2), 518−525.

(48) Zhang, Y.; Furyk, S.; Sagle, L. B.; Cho, Y.; Bergbreiter, D. E.; Cremer, P. S. Effects of Hofmeister Anions on the LCST of PNIPAM as a Function of Molecular Weight. *J. Phys. Chem. C* **2007**, *111* (25), 8916−8924.

(49) Tavagnacco, L.; Zaccarelli, E.; Chiessi, E. On the Molecular Origin of the Cooperative Coil-to-Globule Transition of Poly(N-Isopropylacrylamide) in Water. *Phys. Chem. Chem. Phys.* **2018**, *20* (15), 9997−10010.

(50) Zajforoushan Moghaddam, S.; Thormann, E. Hofmeister Effect on PNIPAM in Bulk and at an Interface: Surface Partitioning of Weakly Hydrated Anions. *Langmuir* **2017**, *33* (19), 4806−4815.

(51) Schroffenegger, M.; Zirbs, R.; Kurzhals, S.; Reimhult, E. The Role of Chain Molecular Weight and Hofmeister Series Ions in Thermal Aggregation of Poly(2-Isopropyl-2-Oxazoline) Grafted Nanoparticles. *Polymers* **2018**, *10* (4), 451.

(52) Bloksma, M. M.; Bakker, D. J.; Weber, C.; Hoogenboom, R.; Schubert, U. S. The Effect of Hofmeister Salts on the LCST Transition of Poly(2-Oxazoline)s with Varying Hydrophilicity. *Macromol. Rapid Commun.* **2010**, *31* (8), 724−728.

(53) Manoharan, V. N. Molecular Forces and Self Assembly: In Colloid, Nano Sciences and Biology. *Phys. Today* **2011**, *64* (2), 48−48.

(54) Gurau, M. C.; Lim, S.-M.; Castellana, E. T.; Albertorio, F.; Kataoka, S.; Cremer, P. S. On the Mechanism of the Hofmeister Effect. *J. Am. Chem. Soc.* **2004**, *126* (34), 10522−10523.

(55) Kunz, W.; Belloni, L.; Bernard, O.; Ninham, B. W. Osmotic Coefficients and Surface Tensions of Aqueous Electrolyte Solutions: Role of Dispersion Forces. *J. Phys. Chem. B* **2004**, *108* (7), 2398−2404.

(56) Thormann, E. On Understanding of the Hofmeister Effect: How Addition of Salt Alters the Stability of Temperature Responsive Polymers in Aqueous Solutions. *RSC Adv.* **2012**, *2* (22), 8297−8305.

(57) Ganesh, V.; Pal, S. K.; Kumar, S.; Lakshminarayanan, V. Self-Assembled Monolayers (SAMs) of Alkoxycyanobiphenyl Thiols on Gold—A Study of Electron Transfer Reaction Using Cyclic Voltammetry and Electrochemical Impedance Spectroscopy. *J. Colloid Interface Sci.* **2006**, *296* (1), 195−203.

(58) Eissa, S.; Zourob, M. Aptamer- Based Label-Free Electrochemical Biosensor Array for the Detection of Total and Glycated Hemoglobin in Human Whole Blood. *Sci. Rep.* **2017**, *7* (1), 1−8.

(59) Lu, G.; Li, Y.-M.; Lu, C.-H.; Xu, Z.-Z. Corrosion Protection of Iron Surface Modified by Poly(Methyl Methacrylate) Using Surface-Initiated Atom Transfer Radical Polymerization (SI-ATRP). *Colloid Polym. Sci.* **2010**, *288* (14), 1445−1455.

(60) Tan, C.; Dutta, G.; Yin, H.; Siddiqui, S.; Arumugam, P. U. Detection of Neurochemicals with Enhanced Sensitivity and Selectivity via Hybrid Multiwall Carbon Nanotube-Ultrananocrystalline Diamond Microelectrodes. *Sens. Actuators, B* **2018**, *258*, 193−203.

(61) Manohar, A. K.; Bretschger, O.; Nealson, K. H.; Mansfeld, F. The Use of Electrochemical Impedance Spectroscopy (EIS) in the Evaluation of the Electrochemical Properties of a Microbial Fuel Cell. *Bioelectrochemistry* **2008**, *72* (2), 149−154.

(62) Mejri, M. B.; Baccar, H.; Baldrich, E.; Del Campo, F. J.; Helali, S.; Ktari, T.; Simonian, A.; Aouni, M.; Abdelghani, A. Impedance Biosensing Using Phages for Bacteria Detection: Generation of Dual Signals as the Clue for in-Chip Assay Confirmation. *Biosens. Bioelectron.* **2010**, *26* (4), 1261−1267.

(63) Mansfeld, F.; Han, L. T.; Lee, C. C.; Zhang, G. Evaluation of Corrosion Protection by Polymer Coatings Using Electrochemical Impedance Spectroscopy and Noise Analysis. *Electrochim. Acta* **1998**, *43* (19), 2933−2945.

(64) Srivastav, S.; Kant, R. Anomalous Warburg Impedance: Influence of Uncompensated Solution Resistance. *J. Phys. Chem. C* **2011**, *115* (24), 12232−12242.

(65) Pauliukaite, R.; Ghica, M. E.; Fatibello-Filho, O.; Brett, C. M. A. Electrochemical Impedance Studies of Chitosan-Modified Electrodes for Application in Electrochemical Sensors and Biosensors. *Electrochim. Acta* **2010**, *55* (21), 6239−6247.

(66) Umpleby, R. J.; Baxter, S. C.; Chen, Y.; Shah, R. N.; Shimizu, K. D. Characterization of Molecularly Imprinted Polymers with the Langmuir-Freundlich Isotherm. *Anal. Chem.* **2001**, *73* (19), 4584−4591.

(67) Eckermann, A. L.; Feld, D. J.; Shaw, J. A.; Meade, T. J. Electrochemistry of Redox-Active Self-Assembled Monolayers. *Coord. Chem. Rev.* **2010**, *254* (15), 1769−1802.

(68) Li, X.; Shen, L.; Zhang, D.; Qi, H.; Gao, Q.; Ma, F.; Zhang, C. Electrochemical Impedance Spectroscopy for Study of Aptamer-Thrombin Interfacial Interactions. *Biosens. Bioelectron.* **2008**, *23* (11), 1624−1630.

(69) Nguyen, T. Q.; Breitkopf, C. Determination of Diffusion Coefficients Using Impedance Spectroscopy Data. *J. Electrochem. Soc.* **2018**, *165* (14), E826−E831.

(70) Kojima, H.; Tanaka, F. Reentrant Volume Phase Transition of Cross-Linked Poly(N-Isopropylacrylamide) Gels in Mixed Solvents of Water/Methanol. *Soft Matter* **2012**, *8* (10), 3010−3020.